Energy Dissipation and Path Instabilities in Dynamic Fracture of Silicon Single Crystals

T. Cramer,[1] A. Wanner,[2] and P. Gumbsch[1]

[1]*Max-Planck-Institut für Metallforschung, Seestrasse 92, 70174 Stuttgart, Germany*
[2]*Institut für Metallkunde, Universität Stuttgart, Seestrasse 71, 70174 Stuttgart, Germany*

(Received 10 January 2000)

Brittle fracture usually proceeds at crack driving forces which are larger than those needed to create the new fracture surfaces. This surplus can lead to faster crack propagation or to the onset of additional dissipation mechanisms. Dynamic fracture experiments on silicon single crystals reported here show several distinct transitions between different dissipation mechanisms. Cleavage fracture is followed by the propagation of a faceted crack front, which is finally followed by a path instability and the propagation of multiple cracks. The fracture surface qualitatively corresponds to the mirror, mist, and hackle morphology of amorphous materials. However, the corresponding fracture mechanisms, which remain largely unknown in the amorphous materials, can clearly be identified here.

PACS numbers: 62.20.Mk, 46.50.+a

An external load acting on a precracked body exerts a driving force on the crack. This driving force is equivalent to the mechanical energy release per unit crack advance, the energy release rate G [1]. In an ideally brittle material crack extension takes place if the crack is supplied with a driving force larger than the specific energy 2γ required to create the fracture surfaces [1,2]. This threshold driving force is called the critical energy release rate G_c. In general, the driving force is not only a function of the geometry of the body and of the external forces but also a function of the shape, size, and orientation of the crack itself. Hence, the driving force may change and rise to levels well above G_c as the crack length l increases during propagation. Interestingly, such supercritical fracture is observed in many practical cases and, from the experimentalist's point of view, can be realized more easily than crack extension under an approximately constant driving force just above the threshold G_c.

How does the crack respond to a driving force that is significantly larger than required? How is the surplus of supplied energy "spent"? Continuum mechanical considerations have so far only answered these questions for the specific case of a crack propagating along a straight path [3]. According to these considerations, a straight crack is expected to attain increasingly higher velocities for increasing energy release rates. The crack velocity asymptotically reaches an upper bound which is equal to the Rayleigh wave velocity c_R, the velocity of acoustic surface waves. For a straight crack propagating at a velocity v below c_R, the dynamic fracture energy, $\Gamma(v)$, can be expressed as:

$$\Gamma(v) = G(l, \sigma)\left(1 - \frac{v}{c_R}\right), \qquad (1)$$

where the energy release rate $G(l, \sigma)$ is the static, time-independent energy flux into the crack tip which represents the geometry of the specimen and the applied stress σ. In the simplest case, the dynamic fracture energy $\Gamma(v)$ is a constant equal to the specific surface energy 2γ of the two fracture surfaces created by the advancing crack.

Fracture experiments on amorphous materials such as polymethylmetacrylate (PMMA) and glass have revealed that cracks do not propagate faster than about $(0.4-0.5)c_R$ [4,5]. These experiments also show that the fracture surfaces are only smooth and mirrorlike if the driving force is close to G_c. If the driving force is increased and the crack thus exceeds a critical velocity v_c, the fracture surfaces become rougher and exhibit a so-called mist and hackle morphology [6]. Below v_c, Eq. (1) has recently been shown to appropriately describe the observed behavior [7]. Above v_c, microscopic bifurcations were proposed as the explanation for the lower than expected terminal crack velocity [7]. The bifurcations are predicted to result from a dynamic crack branching instability [8].

So far most of the fundamental studies in this field have dealt with *amorphous* materials, where a propagating crack can easily deviate from its original plane and thus form a rough fracture surface due to the absence of long-range order. In contrast, brittle *crystalline* materials exhibit well-defined cleavage planes, which render the formation of a rough fracture surface more difficult. Hence, the following question arises: What is limiting the velocity of cracks in brittle crystalline materials?

The dynamics of fast fracture in brittle crystalline materials has been addressed experimentally only in very few studies. Interestingly, most studies gave significantly higher values of $(0.7-0.9)c_R$ for the terminal crack velocities [9–13]. However, a correlation between the fracture surface morphology and the crack dynamics has not been attempted yet and the origin of the terminal velocity in crystalline materials remains unclear.

The purpose of this paper is to provide a detailed time-resolved analysis of the brittle fracture characteristics of single crystalline silicon and a correlation with the fracture surface morphology. This correlation and the quantitative analysis by continuum theory allows one to clearly identify specific energy dissipating mechanisms.

 0031-9007/00/85(4)/788(4)$15.00 © 2000 The American Physical Society

Dynamic fracture experiments were conducted on commercially available (boron-doped) silicon single crystal plates which were loaded to force a {110} cleavage crack in a $\langle 1\bar{1}0 \rangle$ direction. This cleavage system is known to give almost perfectly flat fracture surfaces [14]. The specimen dimensions were height $H \times$ length $L \times$ thickness $= 150 \times 100 \times 0.75$ mm^3. Crack propagation was initiated from a sawn notch by the application of a monotonically increasing tensile stress. Crack extension was monitored via the change of the electric resistance of a thin metal layer sputter-deposited on one surface of the specimen. These crack extension measurements were calibrated *in situ* by means of a set of conductor lines deposited on the opposite surface of the specimen. More experimental details are given in Ref. [15].

The far-field stress σ at which fracture occurred varied between 4.7 and 15.5 MPa via the geometry of the notch (length l_c and root radius). The energy release rate for our specific specimen geometry is almost constant for $0.4L \leq l \leq 0.9L$ [16]. Within this steady-state regime, the energy release rate is approximately equal to the energy release rate expected for an infinitely wide strip which is given by

$$G_s = \frac{\sigma^2 H(1 - \nu^2)}{2E}, \qquad (2)$$

where $\nu = 0.36$ and $E = 169$ GPa [17] are the effective Poisson ratio and Young's modulus, respectively, for the given crystallographic orientation of our silicon specimens. The energy release rate G_s varies between 7 and 89 J/m^2 for the far-field stresses given above. The overloads G_s/G_c therefore range between 2 and 33 (with $G_c = 2\gamma_{(110)} = 3.4$ J/m^2 [18]).

The dependence of the crack velocity on the crack extension is shown in Fig. 1A for a fracture stress of $\sigma = 6.8$ MPa. A short transient is followed by propagation at almost constant velocity. This steady-state velocity is close to the average velocity v_{av}, defined as the ratio of the crack path, $L - l_c$, and the duration of the fracture process. The instantaneous crack velocity is analyzed as a function of the instantaneous crack driving force via the calculated dependence of the energy release rate on crack length $G(l)$ for the given specimen geometry [16] in Fig. 1B. The crack velocity closely follows the continuum mechanical solution $v(G)$ obtained from inversion of Eq. (1) for $\Gamma = 2\gamma_{(110)}$.

The average crack velocities from all our fracture experiments are compared to the continuum mechanical solution $v(G)$ in Fig. 2A. The measured velocities are again in quantitative agreement with the continuum theory at the lowest energy release rates ($G_s = 7$ J/m^2). At high energy release rates, however, the crack velocity is lower than the continuum mechanical prediction which approaches the Rayleigh wave velocity ($c_R = 4.5$ km/s [15]).

The dynamic fracture energy Γ calculated from Eq. (1) as a function of G_s and v_{av}, is displayed in Figs. 2B and 2C. The fracture energy increases linearly with G_s

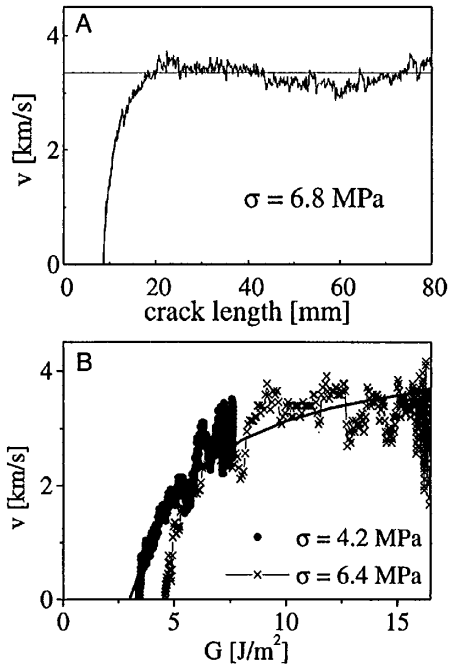

FIG. 1. (A) Measured instantaneous crack velocity v as a function of the crack length. (B) Dependence of the measured crack velocity on crack driving force is compared to the theoretical prediction from Eq. (1) for two specimens fractured at relatively low applied stress.

(Fig. 2B) at high energy release rates. Following Eq. (1) the slope of the $\Gamma(G)$ curve is given by $(c_R - v_t)/c_R$, which uniquely defines a terminal crack velocity $v_t = 3800$ m/s $= 0.85c_R$. The $\Gamma(v)$ curve (Fig. 2C) correspondingly shows a sharp increase as the terminal velocity is approached.

Two important conclusions can be drawn from the experimental results so far. The first is that the continuum mechanical solution for the propagating crack describes the situation at low loads with good accuracy. The second conclusion is that the dynamics of crack propagation at higher energy release rates does not seem to follow the dynamics of a single crack which consumes energy only for the creation of new fracture surface. Nevertheless, the continuum solution can be applied to calculate the energies related to the additional dissipation mechanisms.

The fracture surface morphologies of the specimens were analyzed on a large range of length scales using different microscopical methods. At the lowest fracture stress, corresponding to $G = 7$ J/m^2 and marked with the open circle in Fig. 2, the fracture surface is smooth and mirrorlike. It corresponds to the (110) cleavage plane and remains mirrorlike and featureless down to length scales well below 5 nm as observed by atomic force microscopy (AFM). At higher energy release rates $G \leq 14$ J/m^2 and above crack velocities of $v_{\mathrm{av}} = 3000$ m/s $= (2/3)c_R$ (triangles in Fig. 2) the fracture surface still appears mirrorlike when observed by light optical microscopy. However, AFM reveals that the crack partially deviated from the

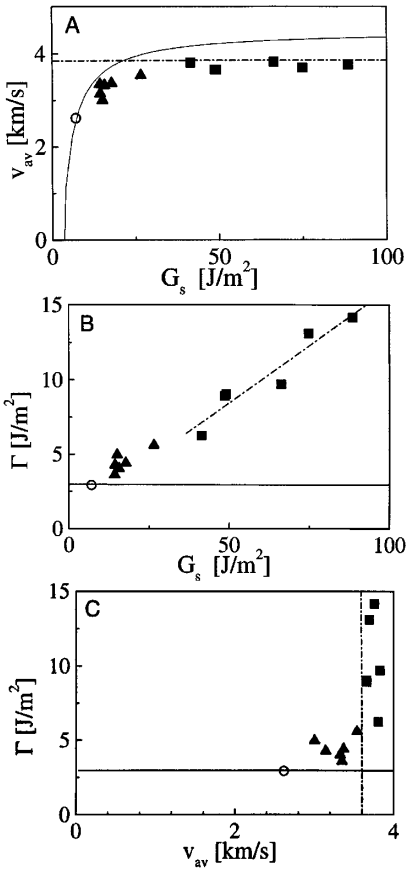

FIG. 2. (A) Average crack velocity v_{av} as a function of the steady state energy release rate G_s. The fracture surface is smooth and mirrorlike over the entire crack path for the specimen fractured at the lowest G_s (open circle). A faceted fracture surface is observed at higher G_s (triangles). At the highest G_s, the fracture surface is very rough (squares). The full line corresponds to the continuum mechanical solution obtained from Eq. (1) using $\Gamma = 3$ J/m^2. Equation (1) is used to determine the fracture energy Γ as a function of (B) the energy release rate G_s or (C) the average velocity v_{av}.

initial (110) plane and displays hills and valleys extending in the crack propagation direction. Similar features are observed in the initial transient mirrorlike region on the fracture surfaces of the specimens fractured at higher fracture loads which clearly faceted on {111} planes towards the end of the mirror zone (Fig. 3).

Crack propagation eventually becomes unstable at $G > 40$ J/m^2 and at velocities close to the terminal velocity (squares in Fig. 2). The instability manifests itself in the onset of pronounced surface features. In this "hackle" region the typical structure size is of the order of $1-200$ μm. The transition from the mirror to the hackle zone is abrupt and the different zones can clearly be distinguished. The hackle region appears to start from the specimen sides and expands gradually into the interior. The fracture surface shows an extended region where parts of the crack front produced mirror and other parts of the crack front produced hackle zones (Fig. 4A). The hackle region itself is characterized by an alternate change of rough structures and

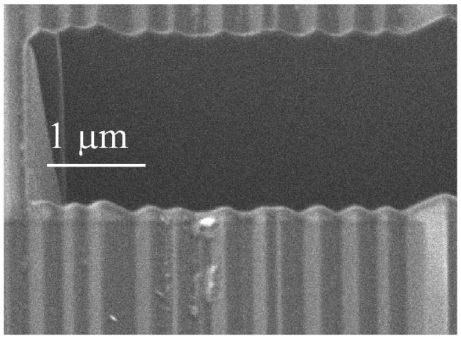

FIG. 3. Trench cut into the end of the mirror zone of a specimen fractured at $G_s = 41$ J/m^2 using a focussed ion beam (FIB). The crack propagated from the bottom to the top of the image on {111} cleavage facets.

relatively smooth planes which extend in the crack propagation direction. Most of the smooth planes are inclined by an angle of about 35° against the (110) cleavage plane, which indicates that they result from cleavage on {111} facets. Rough, nonplanar structures always link two cleavage facets which appear to have simultaneously propagated with two independent crack fronts on different height levels (e.g., Fig. 4B). This suggests that the material placed between the two crack fronts has probably sheared-off far behind the primary crack front. A very clear example of such a secondary shear fracture is shown at higher magnification in Fig. 4C, where even subsurface cracks on the {111} planes can be resolved. The surface features observed in the hackle region are described in more detail in Ref. [15].

This fracture surface analysis shows that there is no unique fracture mode for one crack velocity. Mirror and hackle zones coexist on large sections of the fracture surfaces. There is, however, a unique set of fracture modes and crack velocities for a given overload. Three modes of crack propagation can be distinguished for silicon loaded along the [110] axis so as to advance the crack in a $[1\bar{1}0]$ direction. First, brittle crack propagation of one single crack on the (110) cleavage plane is observed. This case

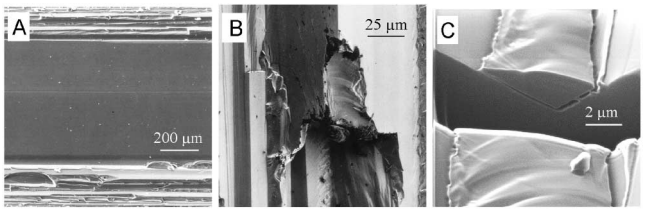

FIG. 4. (A) Scanning electron microscopy (SEM) micrograph showing the coexistence of hackle regions at the sides and a mirror region in the center of the fracture surface. Crack propagation was from left to right. (B) SEM and (C) FIB micrographs show typical features of the hackle region at higher magnification. The trench in (C) has been cut into the fracture surface by a FIB. Subsurface {111} cleavage cracks are clearly visible. The crack propagated from top to bottom in (B) and (C).

is fully described by the continuum mechanical solution, Eq. (1), under the assumption of a constant fracture energy which corresponds to the surface energy of the two (110) surfaces. Second, at intermediate overloads the crack propagates on two sets of {111} planes, which results in a faceted fracture surface and leads to the increased fracture energy (triangles in Fig. 2). The size of the facets increases with increasing G. Because the faceting does not change the total surface energy significantly [$\frac{\gamma_{(111)}}{\cos(35^\circ)} \approx \gamma_{(110)}$ [19]], it is concluded that the crack must spend the additional energy by emitting phonons. Whether this radiation is connected with the formation of the rims between the two {111} fracture surfaces or whether it is connected with the mixed mode I-III loading on the {111} facets is unclear. The onset of the faceting can not be identified on the fracture surfaces, which indicates that the faceting may grow continuously out of small disturbances of a planar crack.

The third mode is only observed at the highest overloads, where the specimens exhibit rough hackle zones. The abrupt onset of the hackle zone is clearly connected with the onset of crack path instabilities. The path instability is apparently connected with the ability of the cracks on the {111} facets to overgrow each other. This locally results in the simultaneous propagation of two crack fronts and in secondary shear fracture of the material placed between. This fracture mechanism exhibits several ways of energy dissipation. Not only is the total surface area increased significantly, but unsteady propagation of the crack front must also be accompanied by significant "noise" and radiation. Hence, the observation that the crack velocity does not increase beyond $0.85c_R$ even at energy release rates as high as $30G_c$ clearly displays the ability of this fracture mechanism to dissipate enormous amounts of energy.

Coming back to the initial question, how does a crack respond to large driving forces? The results presented here show that the crack makes use of all possible ways to spend energy. Initially the easiest way to spend energy is to run faster. Faceting then apparently allows to spend some more energy and finally a very high driving force leads to a path instability which splits the initially continuous crack front and results in the propagation of multiple cracks. This path instability bears some similarity with the bifurcation instability found in PMMA [7]. The terminal velocity at which the instability occurs is of course determined by the material and its crystallographic orientation. One could argue that a low terminal velocity is expected if alternative fracture paths are easily accessible as they are in isotropic amorphous glass or PMMA. Inversely, for a material with only one type of cleavage system like GaAs, where the {110} planes are the only cleavage planes, one would expect to reach very high terminal velocities before the crack can make use of alternative paths.

In general, the dynamic fracture process can be separated into two different regimes: a first regime at low overloads, where the behavior of the crack is material-independent in the sense that it is fully described by linear elastic continuum mechanics once the surface energy and the elastic properties of the material are known, and a second regime, where material-specific dissipation processes dominate. Future investigation must focus on the mechanisms which govern the latter to further advance our understanding of catastrophic failure in materials.

Financial support from Deutsche Forschungsgemeinschaft through grant Gu 367/8 is gratefully acknowledged.

[1] R. Thomson, in *Solid State Physics,* edited by H. Ehrenreich and F. Seitz (Academic Press, New York, 1986), Vol. 39, p. 2.
[2] A. A. Griffith, Philos. Trans. R. Soc. London A **221**, 163 (1920).
[3] L. B. Freund, *Dynamic Fracture Mechanics* (Cambridge University Press, New York, 1990).
[4] J. Fineberg *et al.,* Phys. Rev. Lett. **67**, 457 (1991).
[5] S. P. Gross *et al.,* Phys. Rev. Lett. **71**, 3162 (1993).
[6] J. W. Johnson and D. G. Holloway, Philos. Mag. **14**, 731 (1966).
[7] E. Sharon and J. Fineberg, Nature (London) **397**, 333 (1999).
[8] E. H. Yoffe, Philos. Mag. **42**, 739 (1951).
[9] J. J. Gilman, J. Appl. Phys. **27**, 1262 (1956).
[10] D. Hull and P. Beardmore, Int. J. Fract. Mech. **2**, 468 (1966).
[11] J. E. Field, Contemp. Phys. **12**, 1 (1971).
[12] J. E. Hauch *et al.,* Phys. Rev. Lett. **82**, 3823 (1999).
[13] T. Cramer, A. Wanner, and P. Gumbsch, Phys. Status Solidi (a) **164**, R5 (1997).
[14] G. Michot, Cryst. Prop. Prep. **17–18**, 55 (1988).
[15] T. Cramer, A. Wanner, and P. Gumbsch, Z. Metallkd. **90**, 675 (1999).
[16] T. Cramer, P. Gumbsch, and A. Wanner, in *Werkstoffwoche '98, Bd. X,* edited by W. Muster, J. Zieps, and R. Link (Wiley-VCH, Weinheim, 1998), p. 23.
[17] W. A. Brantley, J. Appl. Phys. **44**, 534 (1973).
[18] R. Pérez and P. Gumbsch, Phys. Rev. Letters **84**, 5347 (2000).
[19] S. B. Bhaduri and F. F. Y. Wang, J. Mater. Sci. **21**, 2489 (1986).